Available online at www.sciencedirect.com
SCIENCE DIRECT®
Journal of Sound and Vibration 264 (2003) 707–731
JOURNAL OF SOUND AND VIBRATION
www.elsevier.com/locate/jsvi

Design and analysis of a scaled model of a high-rise, high-speed elevator

W.D. Zhu[a,*], L.J. Teppo[b]

[a] *Department of Mechanical Engineering, University of Maryland Baltimore County, 1000 Hilltop Circle, Baltimore, MD 21250, USA*

[b] *SPARTA , Inc., 1911 N. Fort Myer Drive, Suite 1100, Rosslyn, VA 22209, USA*

Received 15 August 2001; accepted 19 July 2002

Abstract

A novel scaled model is developed to simulate the linear lateral dynamics of a hoist cable with variable length in a high-rise, high-speed elevator. The dimensionless groups used to formulate the scaling laws are derived through dimensional analysis. The model parameters are selected based on the scaling laws and are subject to the material, size, and hardware constraints. It is demonstrated that while it is impossible to obtain a fully scaled model unless the model is extremely tall, a reasonably sized model can be designed and the scaling laws that are not satisfied can be rendered to have a minimal effect on the scaling between the model and prototype. In conjunction with the model design, an analysis of model tension in a closed band loop is developed. A new movement profile that ensures a continuous jerk function during the entire period of motion is derived. The dynamic response of the prototype cable and that of the model band under consideration are compared numerically. Practical considerations that occur in the design of the model are addressed. The methodology can be used to investigate the vibration of a very long cable in other applications.

1. Introduction

The advent of high-rise buildings in modern cities requires high-speed elevator systems to provide quick access within buildings. Before the world's tallest buildings, the 452-m Petronas Twin Towers, were completed in Malaysia in 1998, work had begun on the 460-m Shanghai World Financial Center in China. This upward trend is expected to continue in the new millennium with buildings over 500 m being planned [1]. Developing roped elevator technology for tall buildings poses significant challenges. To improve the efficiency, it is necessary to increase

*Corresponding author. Tel.: +1-410-455-3394; fax: +1-410-455-1052.
E-mail address: wzhu@umbc.edu (W.D. Zhu).

0022-460X/03/$ - see front matter © 2002 Elsevier Science Ltd. All rights reserved.
doi:10.1016/S0022-460X(02)01218-X

the current speed limit of 750 m/min up to 1000 m/min in the future. However, the acceptable levels of vertical and lateral vibrations for high-speed elevators are very small and typically expressed in millG target levels (e.g., 8–10 millG) [1]. While there is no limit to the velocity at which a passenger can tolerate in an elevator car, acceleration is often limited to $1\,m/s^2$ and jerk (rate of change of acceleration) $1.5\,m/s^3$. The performance requirements for high-rise elevators are also very stringent; the vertical positioning accuracy is typically within the range of 0.001–0.005% of the full range of motion (e.g., 6 mm for rises up to 500 m) [1]. To meet these design challenges, one of the major tasks is to develop an improved understanding of elevator cable dynamics. Unlike low-rise towers, cable dynamics plays an important role in system modelling of high-rise elevators.

Research on modelling the elevator cable dynamics has been limited in the literature. Chi and Shu [2] calculated the natural frequencies associated with the longitudinal vibration of a stationary hoist cable coupled with the vertical vibration of an elevator car. Yamamoto et al. [3] analyzed the free and forced lateral vibrations of a stationary string with slowly, linearly varying length. Terumichi et al. [4] examined the lateral vibration of a travelling string with slowly, linearly varying length and a mass–spring termination. General energy and stability characteristics of horizontally and vertically translating beams and strings with arbitrarily varying length and various boundary conditions were studied in Ref. [5]. While the amplitude of the response can behave in a different manner, the energy of vibration of translating media decreases and increases in general during extension and retraction, respectively. This explains the "unstable shortening cable behavior" encountered in the elevator industry. An active control methodology using a pointwise control force and/or moment was developed by Zhu et al. [6] to dissipate vibratory energies of translating media with variable length. Optimal control gains, leading to the fastest rates of decay of vibratory energies of a translating beam during extension and retraction, were identified.

The aim of this paper is to design a novel scaled model to simulate the linear lateral dynamics of a travelling cable with variable length in a high-rise, high-speed elevator. Because it is not practical to build a full-scale elevator system for every possible test configuration, a carefully scaled model can be designed within limiting factors to give a good look at the prototype behavior. It provides a convenient and cost-effective means for predicting the full-scale behavior from experiments on a small-scale model in the laboratory. To this end, the Buckingham pi theorem [7] is used to form the dimensionless groups. The scaling laws used to design the model are formulated. In conjunction with the model design, a statically indeterminate analysis of model tension in a closed band loop is presented. Practical issues that arise in the design of the model, including friction modelling and band slip control, are addressed. A new movement profile, ensuring a continuous jerk function in the entire period of motion, is derived. The dynamic response of the prototype cable, represented by the model band, is obtained using a modified Galerkin's method [5] and compared to its actual response.

2. Description of the prototype

The prototype elevator considered here is an idealized, high-speed elevator travelling the first 50 stories in a 57-story building. Each story is assumed to be 3 m. Hence the length of the elevator movement is 150 m with the cable length above the elevator car at the end of its movement being

21 m. It is assumed that the maximum velocity of the car is 5 m/s, and the maximum acceleration is 0.75 m/s^2. Six identical, parallel, hoist cables are used to suspend the elevator car of mass 4536 kg from the drive sheave at the top of the building. Each cable, with linear density 1.005 kg/m and bending rigidity 1.39 N/m^2, is assumed to support one-sixth of the total load. When the car is stationary, the tension in each cable is 7414 N at the top of the elevator car and increases linearly to the top of the cable due to cable weight. Since the lateral vibrations of each hoist cable around its straight equilibrium are assumed to be small, the longitudinal and lateral vibrations of the cable are uncoupled within the linear theory. Similarly, the lateral vibrations of the cable in the two planes are assumed to be uncoupled. The friction forces in the prototype elevator are assumed to be negligible as they are small components of the cable tensions. While the lateral vibration of each cable in one plane, during the upward movement of the elevator car, is modelled in this work, the methodology can be extended to investigate its longitudinal vibration. We study the upward movement of the elevator here because its hoist cables are characterized by an inherent instability during retraction [5] and the efficacy of the control method in Ref. [6] in dissipating their vibratory energies can be assessed experimentally. In the model designed here, the suspensions of the car against the guide rails are assumed to be rigid. The key parameters used for the prototype elevator are summarized in Table 1. Note that the subscripts p and m denote prototype and model, respectively, throughout this paper.

The prototype elevator is driven by a motor connected to the sheave at the top of the elevator shaft. Each cable passes over an idler sheave and is attached to a counterweight (Fig. 1). The purpose of the counterweight is to offset the weight of the elevator and reduce the torque on the motor when the elevator is stationary or moving at constant velocity. In order to accelerate the car upward, the motor must supply additional torque to the sheave. This increases the tensions in the cables above the car and decreases the tensions in the cables above the counterweight. The net result is that the motor must provide enough additional torque to accelerate the entire inertia of the system, including the elevator car, counterweight, cables, and drive sheave (see Section 5.1). The segment of each cable of interest is modelled as a translating, tensioned beam with fixed boundaries. Because the bending rigidity of the cable is small relative to its tension and the supporting sheave is almost rigid, the lateral vibration of the segment of the cable under consideration is assumed to be uncoupled from that of its adjacent segment.

Table 1
Key prototype parameters

Parameter	Description	Value
l_{0p}	Cable length above the elevator car at the start of movement	171 m
l_{endp}	Cable length above the elevator car at the end of movement	21 m
m_{ep}	Mass of one-sixth of the elevator car	756 kg
T_{0p}	Nominal cable tension at the top of the elevator car	7414 N
ρ_p	Mass per unit length of the cable	1.005 kg/m
v_{maxp}	Maximum velocity of the elevator car	5 m/s
a_{maxp}	Maximum acceleration of the elevator car	0.75 m/s^2
$(EI)_p$	Bending rigidity of the cable	1.39 Nm^2
g	Gravitational acceleration	9.81 m/s^2

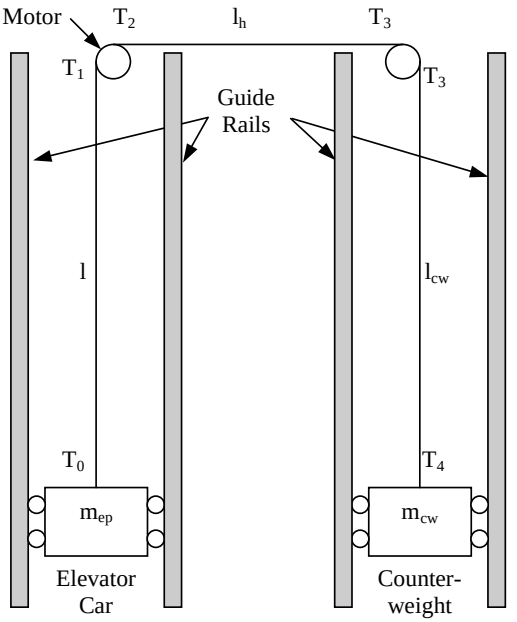

Fig. 1. Schematic of the prototype elevator. The lengths of three cable segments shown are denoted by l, l_h, and l_{cw}. The tensions at the two ends of each cable segment are denoted by T_0–T_4.

3. Dimensional analysis

With respect to the inertial x-axis from the drive sheave to the car, the linear equation, governing the free lateral vibration of the segment of the cable under consideration about its static equilibrium, is [5]

$$\rho[y_{tt} - 2v(t)y_{xt} + v^2(t)y_{xx} - a(t)y_x] - [T(x,t)y_x]_x + EIy_{xxxx} = 0, \quad 0 < x < l(t), \tag{1}$$

where the subscripts denote partial differentiation, $y(x,t)$ is the lateral displacement of the cable particle instantaneously located at spatial position x at time t, ρ is the mass per unit length of the cable, EI is its bending rigidity, $T(x,t)$ is the cable tension at position x at time t, $l(t)$ is the prescribed length of the cable at time t, and $v(t) = -\dot{l}(t)$ and $a(t) = -\ddot{l}(t)$ are the prescribed velocity and acceleration of the car, respectively. Note that the minus signs in the above expressions for $v(t)$ and $a(t)$ indicate that the upward direction is the positive direction of motion for the car. The initial displacement and velocity of the cable are specified along the spatial domain $0 < x < l_0$, where l_0 is the initial cable length. The tension in the cable, which varies linearly along its length, is [5]

$$T(x,t) = T_0 + \Delta T_g(x,t) + \Delta T_a(x,t), \tag{2}$$

where T_0 is the nominal cable tension at the top of the car when the elevator is stationary or moving at constant velocity, ΔT_g is the tension change due to cable weight, and ΔT_a is the tension change due to acceleration. They are given by

$$T_0 = m_e g, \quad \Delta T_g = \rho[l(t) - x]g, \quad \Delta T_a = [m_e + \rho(l(t) - x)]a(t), \tag{3}$$

where m_e is the mass of one-sixth of the elevator car and g is the acceleration due to gravity. Excluding the initial conditions, the lateral vibration of the cable can be described as a function f of 11 variables:

$$y = f(x, t, l_0, l(t), v(t), a(t), \rho, EI, T_0, g, m_e). \tag{4}$$

Note that T_0 is included as an independent variable in Eq. (4) because extra tension, in addition to the car weight, often needs to be applied to the model (see Section 4).

The twelve dimensional variables in Eq. (4) can be converted into nine dimensionless groups using the Buckingham pi theorem. The repeating parameters selected to form the dimensionless groups are l_0, ρ, and T_0, because they are easily measured constants and contain the three basic dimensions that need to be scaled: length, mass, and time. Through a standard procedure [7], the following dimensionless pi terms are obtained:

$$\begin{gathered} \Pi_1 = \frac{y(x,t)}{l_0}, \quad \Pi_2 = \frac{x}{l_0}, \quad \Pi_3 = \frac{t}{l_0}\sqrt{\frac{T_0}{\rho}}, \quad \Pi_4 = \frac{l(t)}{l_0}, \quad \Pi_5 = v(t)\sqrt{\frac{\rho}{T_0}}, \\ \Pi_6 = a(t)\frac{\rho l_0}{T_0}, \quad \Pi_7 = \frac{EI}{T_0 l_0^2}, \quad \Pi_8 = \frac{g l_0 \rho}{T_0}, \quad \Pi_9 = \frac{m_e}{l_0 \rho}. \end{gathered} \tag{5}$$

Note that the dimensionless pi terms in Eq. (5) can also be obtained by non-dimensionalizing the governing equation in Eq. (1). The dimensionless displacement of the cable can be expressed as a function F of eight dimensionless variables Π_2–Π_9:

$$\Pi_1 = F(\Pi_2, \Pi_3, \ldots, \Pi_9). \tag{6}$$

4. Scaling laws and model design

If the pi terms Π_{2m} , Π_{3m} , …, Π_{9m} of the model equal the corresponding pi terms Π_{2p}, Π_{3p}, …, $\Pi_{9\mathrm{p}}$ of the prototype, Π_{1m} will equal Π_{1p} and the model and prototype will be completely similar. The first six pi terms in Eq. (5) are not constants; they indicate how the amplitude of vibration of the cable particle under consideration, its spatial location, time, cable length, car velocity, and car acceleration correspond between the model and prototype, respectively. The remaining three pi terms describe the scaling of the bending rigidity (Π_7), the tension change due to gravity (Π_8), and the tension change due to acceleration (Π_9) between the model and prototype.

The Π_2 through Π_6 terms can be fully scaled between the model and prototype. Setting $\Pi_{3p} = \Pi_{3m}$ yields

$$t_m = t_p \frac{l_{0m}}{l_{0p}} \sqrt{\frac{T_{0p}\rho_m}{T_{0m}\rho_p}}. \tag{7}$$

This allows calculation of times in the model that correspond to those in the prototype. Setting $\Pi_{5p} = \Pi_{5m}$ gives the relationship between the transport speeds of the model and prototype elevators:

$$v_m(t_m) = v_p(t_p) \sqrt{\frac{T_{0m}\rho_p}{T_{0p}\rho_m}}. \tag{8}$$

Using the parameters in Table 1, the prototype values for the last three pi terms in Eq. (5) are

$$\Pi_{7p} = 6.4 \times 10^{-9}, \quad \Pi_{8p} = 0.2, \quad \Pi_{9p} = 5.0. \tag{9}$$

Note that $\Pi_{8p}\Pi_{9p} = 1$ because $T_0 = m_e g$ for the prototype. When the weight of the model car alone does not provide enough tension required by the scaling laws, external tension needs to be applied to the model and Π_{8m} becomes independent of Π_{9m}. To match the Π_{7p} term of the prototype, the model cable must have a small bending rigidity $(EI)_m$ and a high nominal tension T_{0m}. As predicted by Eqs. (7) and (8), a larger mass density ρ_m results in a slower time scale and transport speed for the model, which can lead to reduction of the sampling rates and enhance the experiments on the model cable. A flat band was chosen for the model cable because its area moment of inertia I_m is considerably smaller than that of a round cable for a given ρ_m. It can also constrain the lateral vibration of the cable to a single plane for model validation purposes. The choice of band thickness can significantly influence the scaling of the model. Reducing the band thickness by half reduces I_m by a factor of 8 and ρ_m by half. In order to maintain the same time scale and transport speed for the model, the nominal tension T_{0m} can be reduced by a factor of two. This will result in a net reduction of the Π_{7m} term by a factor of four. Decreasing the width of the band, however, will decrease I_m and Π_m by the same factor. Maintaining the same values for t_m and v_m in Eqs. (7) and (8) requires reduction of T_{0m} by half, yielding no net change in the Π_{7m} term. While decreasing the band tension can facilitate the model experiments as indicated earlier, it can adversely affect the scaling of Π_7 and cause band slippage on the motor pulley. The band material can be selected to have a low modulus of elasticity E_m and a high linear density ρ_m. Gold appears to be one of the best choices, but it will incur a high cost. While copper and brass are good alternatives because they have lower modulus of elasticity and slightly higher linear density than steel, a steel band of width 12.7 mm, thickness 0.38 mm, and modulus 207 GPa was used in the model because it is readily available. The linear density and bending rigidity of the band are

$$\rho_m = 0.0392\text{kg/m}, \quad (EI)_\text{m} = 1.20 \times 10^{-2}\text{Nm}^2. \tag{10}$$

Since the acceleration of gravity is the same for the model and prototype, setting $\Pi_{8p} = \Pi_{8m}$ yields

$$T_{0m} = T_{0p}\frac{l_{0m}\rho_m}{l_{0p}\rho_p}. \tag{11}$$

Setting $\Pi_{7p} = \Pi_{7m}$ and using Eq. (11) yields

$$l_{0m} = l_{0p}\sqrt[3]{\frac{\rho_p(EI)_m}{\rho_m(EI)_p}}. \tag{12}$$

Setting $\Pi_{9p} = \Pi_{9m}$ yields

$$m_{em} = m_{ep}\frac{l_{0m}\rho_m}{l_{0p}\rho_p}. \tag{13}$$

Substituting the prototype values in Table 1 and model values in Eq. (10) into Eqs. (11)–(13) yields $T_{0m} = 175$ N, $l_{0m} = 103.4$ m, and $m_{em} = 17.84$ kg. Since l_{0m} is much too high for a model, it is impossible to satisfy the scaling laws associated with the Π_7–Π_9 terms unless the model is

extremely tall. However, a reasonably sized model can be designed, with the Π_7–Π_9 terms rendered to have a secondary effect on the scaling between the model and prototype.

Since Π_{7p} in Eq. (9) is extremely small, an attempt was made to render the Π_{7m} term as small as possible subject to the space, motor speed, and sampling rate constraints. The model elevator car is able to travel 2.2 m with 0.31 m of band between the car and band guide (see Fig. 2) at the end of travel. The band guide consists of two flat steel bars pressed against the band and lubricated with silicon/teflon spray lubricant. This gives the band a fixed boundary condition at the band guide. The use of the band guide can also isolate the vibration of the segment of the band of interest from its adjacent segment. The position where the band passes between the steel bars corresponds to the point of contact between the cable and sheave in the prototype elevator. A servomotor, with a maximum rotational speed of 1120 r.p.m., is used to run the model. It is mounted on a 65 mm diameter motor pulley, which allows a maximum elevator velocity of 3.76 m/s. To avoid running the motor at its absolute maximum speed, a maximum motor speed of 1050 r.p.m. is used, which yields a maximum elevator velocity v_{maxm}=3.53 m/s. Using Eq. (8) yields

$$T_{0m} = T_{0p}\frac{v_{maxm}^2\rho_m}{v_{maxm}^2\rho_p}. \tag{14}$$

Substituting the prototype and model values into Eq. (14) yields $T_{0m} = 144$ N. Hence $\Pi_{7m} = 1.3 \times 10^{-5}$ and $\Pi_{8m} = 0.007$. The effects of dimensionless bending rigidity on the natural frequencies of the prototype and model cables are estimated in Appendix A. Setting $\Pi_{5m} = \Pi_{5p}$ yields the maximum acceleration of the model $a_{maxm} = 25.4\,\text{m/s}^2$.

The choice of the model car mass has an effect on the power of the driving motor and the scaling of the tension change due to acceleration (see Section 5.2). The mass of the current model

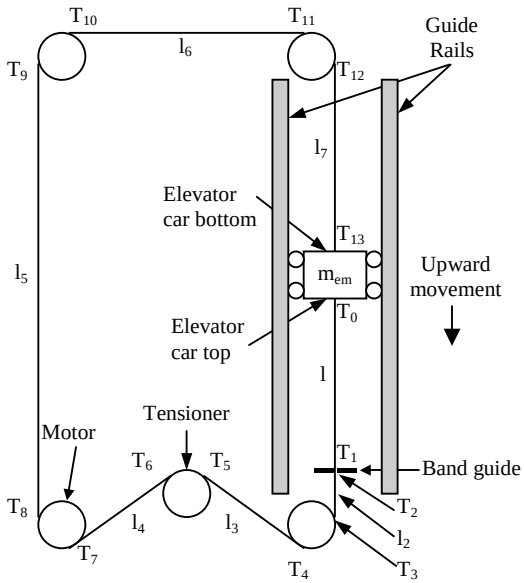

Fig. 2. Schematic of the model elevator. The lengths of seven band segments shown are denoted by l and l_2–l_7. The tensions at two ends of each band segment are denoted by T_0–T_{13}. The model is inverted with "upward" movement of the band between the car and band guide corresponding to its decreasing length l.

car, including that of an actuator attached to the car for future control experiments, is 1.17 kg. Since the weight of the car is far smaller than the nominal model tension required, a continuous band loop, along with a tensioning pulley (see Fig. 2), were designed to provide appropriate overall tension. Because the tension in the closed band loop has different characteristics from that in the prototype, as shown in Section 5, the scaling of the tension change due to acceleration between the model and prototype is no longer governed by Π_9.

As indicated by the Π_8 term in Eq. (5), scaling the tension change due to cable weight would require an extremely dense band material, a large increase in model height, or a decrease in band tension. The effect associated with each has been discussed earlier. In the prototype elevator, when the car is at the start of upward movement with constant velocity, the cable tension varies linearly from 7414 N at the car to 9099 N at the sheave, which is an increase of 22.7%. When the car is at the end of upward movement with constant velocity, the cable tension is 2.8% higher at the sheave than that at the car. In the model, the maximum weight of the band between the car and band guide is 0.96 N, so there is only a 0.7% maximum increase of tension due to band weight. Because the tension change due to band weight is so small, the model can be run upside-down, as shown in Fig. 2, with the "upward" movement of the band between the car and band guide corresponding to its decreasing length. This changes the value of Π_{8m} to -0.007. References to the "top" of the car in what follows mean the side closest to the floor of the building. The band was bolted to the top of the car, giving it a fixed boundary condition. The inversion of the model offers two advantages. First, it allows easier placement of and access to the actuator and sensors in the control experiments to be conducted in the future. Second, it can reduce band slip because during acceleration the weight of the car acts in the same direction as acceleration, and during deceleration the friction force between the car and guide rails helps decelerate the system. The counterweight is not used here in the model in order to reduce the total inertia of the system, and consequently, band slippage. Table 2 summarizes the key design parameters of the model elevator.

5. Analysis of cable tensions in prototype and model elevators

The cable tensions in the prototype and model elevators are analyzed here. The tension changes due to acceleration in both cases are estimated and compared.

Table 2
Key model parameters

Parameter	Description	Value
l_{0m}	Band length between the elevator car and band guide at the start of movement	2.51 m
l_{endm}	Band length between the elevator car and band guide at the end of movement	0.31 m
m_{em}	Mass of the elevator car	1.17 kg
T_{0m}	Nominal band tension at the top of the elevator car	144 N
ρ_m	Mass per unit length of the band	0.0392 kg/m
v_{maxm}	Maximum velocity of the elevator car	3.53 m/s
a_{maxm}	Maximum acceleration of the elevator car	25.4 m/s^2
$(EI)_m$	Bending rigidity of the band	1.20×10^{-2} N m^2
g	Gravitational acceleration	9.81 m/s^2

5.1. Prototype elevator

If the motor is holding the prototype elevator in Fig. 1 stationary, the tensions at the ends of all the cable segments are

$$T_0 = m_{ep}g, \quad T_1 = \rho_p g l + T_0, \quad T_2 = T_3, \quad T_3 = \rho_p l_{cw} g + T_4, \quad T_4 = m_{cw}g, \tag{15}$$

where m_{cw} is the mass of one-sixth of the counterweight and l_{cw} is the length of the cable between the idler sheave and counterweight. It can be seen from Eq. (15) that the difference in tension across the motor is

$$T_1 - T_2 = [m_e - m_{cw} + \rho_p(l - l_{cw})]g, \tag{16}$$

which is maintained by the friction force of the cable on the sheave. To hold the elevator in position, the motor applies a constant torque equal to the tension difference in Eq. (16) times the radius of the motor sheave. Because the friction forces in the prototype elevator are neglected, the tensions in the cable during constant velocity movement are given by the same expressions as those in Eqs. (15)–(16).

To accelerate the elevator upward at rate a, the motor must apply an additional torque to the sheave that is transmitted by friction to the cable, which increases T_1 and decreases T_2. Because the stretch of the cable is not considered, the elevator car, cable, and counterweight must accelerate at the same rate. With moments of inertia of the idler sheave and segment of the cable around it neglected, the new tensions are

$$\begin{aligned} &T_{0a} = m_{ep}(g + a), \quad T_{1a} = \rho_p l(g + a) + T_{0a}, \quad T_{2a} = -\rho_p l_h a + T_{3a}, \\ &T_{3a} = \rho_p l_{cw}(g - a) + T_{4a}, \quad T_{4a} = m_{cw}(g - a), \end{aligned} \tag{17}$$

where the subscript a denotes acceleration and l_h is the length of the cable between the drive and idler sheaves. The new difference in tension across the motor is

$$T_{1a} - T_{2a} = [m_{ep} - m_{cw} + \rho_p(l - l_{cw})]g + [m_{ep} + m_{cw} + \rho_p(l + l_h + l_{cw})]a. \tag{18}$$

It can be seen that the additional tension difference over the stationary or constant velocity case is equal to the acceleration times the total mass of the system.

The additional tensions required at the two ends of the cable of interest to accelerate the system are

$$T_{0a} - T_0 = m_{ep}a, \quad T_{1a} - T_1 = (\rho_p l + m_{ep})a. \tag{19}$$

The tension change due to acceleration at any other point in the cable varies linearly between these two values. Under the movement profile shown in Fig. 4, the tensions at the two ends of the cable under maximum acceleration ($a = 0.75\,\mathrm{m/s^2}$) at time $t = 1.33\,\mathrm{s}$ are $T_{0a} = 7981\,\mathrm{N}$ and $T_{1a} = 9793\,\mathrm{N}$, and those under maximum deceleration ($a = -0.75\,\mathrm{m/s^2}$) at time $t = 36.67\,\mathrm{s}$ are $T_{0a} = 6847\,\mathrm{N}$ and $T_{1a} = 7040\,\mathrm{N}$. The maximum tension changes due to acceleration and deceleration are increases and decreases of 7.6%, respectively, throughout the cable.

5.2. Model elevator

A model elevator consisting of a steel frame approximately 3 m tall was constructed. The model configuration is shown in Fig. 2, with l and l_i ($i = 2, 3, \ldots, 7$) denoting the lengths of corresponding

band segments and T_i ($i=0, 1, \ldots, 13$) the tensions at the ends of all the band segments. The model tower consists of two sub-systems: the support structure and the guide rail system. The guide rails were disjointed from the main support structure to isolate structural vibration from the motor to the band, car, and guide rails. Chrome steel hydraulic cylinders were used as guide rails to provide the straightness, rigidity, and smoothness of operation required. They are 25.4 mm in diameter and set 152 mm apart. Supported on a float plate, the guide rails are adjustable, which can reduce the risk of car "jamming" during its travel. The elevator car is a block of aluminum with two linear bearings that slide on the guide rails. The bearings are assumed to be rigid. A tensioning pulley was designed on a tension plate. Threaded rods with nuts move the plate upward and downward to adjust the tension in the band.

Unlike the prototype elevator, the friction forces in the model are considered because they can constitute a significant fraction of the model tension. When the model is in motion, the kinetic frictions at the elevator car, band guide, and pulleys are assumed to remain constant. It is further assumed that the idler and tensioning pulleys have the same friction. Because the motor is driving the system, the friction at the motor pulley does not affect the tensions in the band. When the model is at rest, however, the static friction at each location can act in either direction and assume different values. Due to the same frictions, the tensions in the band loop during acceleration are compared to those during constant velocity movement in the same direction. Since the closed band loop is a statically indeterminate system, an additional equation involving the elongation of the band under tension will be used. The key is to find a complete set of tensions in the entire band, from which the total elongation of the band, Δl_t, without considering the elongation of the segment of the band that wraps around each pulley, can be calculated. Since the model frame and pulleys can be assumed to be rigid, this total elongation must remain constant under all motion conditions.

In this analysis, it is assumed that, under constant (slow) velocity, the tension of the band at the top of the car, when the car is at its start position of an upward (toward the band guide) movement, is measured through the use of a strain gage attached to the band. This tension, denoted by T_{0v}, where the subscript v denotes constant velocity, is set to be the nominal tension T_{0m} by adjusting the tensioning pulley. Denote the elevator car friction by F_e, band guide friction by F_g, and pulley friction by F_p, where the pulley friction is expressed as a tension difference across its surface. Since the tension T_{0v} at the start position is specified, the tensions at all the other locations can be determined from

$$\begin{aligned}
&T_{6v} = T_{7v}, && T_{5v} = T_{6v} - F_p, && T_{4v} = T_{5v}, && \\
&T_{3v} = T_{4v} - F_p, && T_{2v} = T_{3v} + \rho_m l_2 g, && T_{1v} = T_{2v} - F_g, && \\
&T_{0v} = T_{1v} + \rho_m l g, && T_{13v} = T_{0v} + m_{em} g - F_e, && T_{12v} = T_{13v} + \rho_m l_7 g, && \\
&F_{11v} = F_{12v} - F_p, && T_{10v} = T_{11v}, && T_{9v} = T_{10v} - F_p, && T_{8v} = T_{9v} - \rho_m l_5 g.
\end{aligned} \tag{20}$$

With the lengths of various band segments and their axial rigidity $(EA)_m$ given, and the friction forces estimated from measurements performed on the model elevator [8], as shown in Table 3 where $l=2.51$ m, the total elongation of the band is calculated to be $\Delta l_t = 0.95$ mm.

When the car reaches any other position ($0.31\,\text{m} \leqslant l < 2.51\,\text{m}$) during constant velocity movement upward, the tensions T_{iv} ($i=0,1, \ldots, 13$) in the band can be determined from Eq. (20) along with an equation constraining the total elongation of the band Δl_t to be 0.95 mm.

Table 3
Additional parameters used to calculate the model tensions

Parameter	Value (m)	Parameter	Value
l_2	0.13	m_l	0.085 kg
l_3	0.23	$(EA)_m$	999000 N
l_4	0.23	F_e	4.9 N
l_5	2.90	F_g	6.2 N
l_6	0.41	F_p	2.7 N
l_7	2.71-l		

The resulting tension at the top of the car is

$$\begin{aligned} T_{0v} = \frac{1}{l_t}\{&(EA)_m \Delta l_t - [(m_{em} + \tfrac{1}{2}\rho_m l_7)g - F_e]l_7 + \tfrac{1}{2}\rho_m g l^2 + [\rho_m(l + \tfrac{1}{2}l_2)g - F_g]l_2 \\ &+ [\rho_m(l + l_2)g - F_g - F_p]l_3 - [F_g + 2F_p - \rho_m(l + l_2)g]l_4 \\ &- [(m_{em} + \rho_m l_7 - \frac{1}{2}\rho_m l_5)g - F_e - 2F_p]l_5 - [m_{em} + \rho_m l_7)g - F_e - F_p]l_6\}, \end{aligned} \tag{21}$$

where $l_t = l + l_2 + l_3 + l_4 + l_5 + l_6 + l_7$ is the sum of all the lengths. While the tension at the top of the car in the prototype remains at 7414 N during constant velocity movement upward, T_{0v} in the model decreases monotonically from 144 N at the start position ($l = 2.51$ m) to 141.4 N at the end position ($l = 0.31$ m). It is seen from Eq. (20) that the tension difference across the motor during constant velocity movement is

$$T_{7v} - T_{8v} = F_g + F_e + 4F_p - m_{em}g + \rho_m(l_5 - l_7 - l_2 - l)g. \tag{22}$$

During acceleration, the tension changes at all the locations in the band over the constant velocity case can be determined. They arise from acceleration of the band, elevator car, and idler and tensioning pulleys. The change in T_7, arising from each individual source, is calculated first and superposed. If the tension change varies linearly across a band segment of length l_i, the resulting change in its elongation is

$$\Delta l_i = \frac{(\Delta T_b + \Delta T_c)l_i}{2(EA)_m}, \tag{23}$$

where ΔT_b and ΔT_c are the tension changes at the two ends of the band segment. If the tension change ΔT is uniform across the band segment, the change in its elongation is

$$\Delta l_i = \frac{\Delta T l_i}{(EA)_m}. \tag{24}$$

To accelerate a band segment of length l_i at rate a, the tension difference across its length is $\rho l_i a$. The tension difference across the motor to accelerate the entire band is

$$\Delta T_7^{band} - \Delta T_8^{band} = \rho_m l_t a. \tag{25}$$

Since the tension change varies linearly across the entire band and the total change in its elongation is zero, using Eqs. (23) and (25) yields

$$\Delta T_7^{band} = -\Delta T_8^{band} = \frac{\rho_m l_t a}{2}. \tag{26}$$

To accelerate the elevator car, the motor will increase the tensions in the band segments with lengths l, l_2, l_3, and l_4, and decrease the tensions in the band segments with lengths l_5, l_6 and l_7. Because the tension changes along the former group of band segments are uniform and equal, they are denoted by ΔT_7^{car}. Similarly, the tension changes along the latter group of band segments are denoted by ΔT_8^{car}. Since the total change of elongation in the entire band must equal zero, we have

$$\frac{\Delta T_7^{car}(l + l_2 + l_3 + l_4)}{(EA)_m} + \frac{\Delta T_8^{car}(l_5 + l_6 + l_7)}{(EA)_m} = 0, \tag{27}$$

where Eq. (24) has been used. Also, the tension difference across the motor to accelerate the car is

$$\Delta T_7^{car} - \Delta T_8^{car} = m_{em} a. \tag{28}$$

Combining Eqs. (27) and (28) yields

$$\Delta T_7^{car} = \frac{m_{em} a(l_5 + l_6 + l_7)}{l_t}. \tag{29}$$

Let r be the radius of each idler or the tensioning pulley, and ΔT_p the tension difference across each pulley to provide its angular acceleration. Setting the torque due to tension difference equal to the angular acceleration of the pulley α times its moment of inertia I gives

$$\Delta T_p r = I\alpha = \left(\tfrac{1}{2} m r^2\right)\frac{a}{r}, \tag{30}$$

where m is the mass of the pulley. Solving Eq. (30) for ΔT_p yields

$$\Delta T_p = \frac{m}{2} a. \tag{31}$$

It can be seen from Eq. (31) that the pulley inertia causes a tension difference equivalent to a linear inertia m_l of half the mass. For aluminum pulleys used in the model with width 0.019 m, radius 0.032 m, and density 2800 kg/m^3, we have m_l=0.085 kg.With the idler and tensioning pulleys treated in the same way as the elevator car and their effects added, one has

$$\Delta T_7^{pulley} = \frac{m_l a[l_3 + 2(l_2 + l + l_7) + 3l_6 + 4l_5]}{l_t}. \tag{32}$$

Summing Eqs. (26), (29), and (32) yields the total change in T_7 due to acceleration:

$$\begin{aligned} \Delta T_7 &= \Delta T_7^{band} + \Delta_7^{car} + \Delta T_7^{pulley} \\ &= \frac{\rho_m l_t a}{2} + \frac{m_{em} a(l_5 + l_6 + l_7)}{l_t} + \frac{m_l a[l_3 + 2(l_2 + l + l_7) + 3l_6 + 4l_5]}{l_t}. \end{aligned} \tag{33}$$

The tension change at any other end point in the band loop is calculated by subtracting from ΔT_7 the amount of tension difference required to accelerate each associated component:

$$\begin{aligned}
&\Delta T_6 = \Delta T_7 - \rho_m l_4 a, \quad \Delta T_5 = \Delta T_6 - m_l a, \quad \Delta T_4 = \Delta T_5 - \rho_m l_3 a,\\
&\Delta T_3 = \Delta T_4 - m_l a, \quad \Delta T_2 = \Delta T_3 - \rho_m l_2 a, \quad \Delta T_1 = \Delta T_2,\\
&\Delta T_0 = \Delta T_1 - \rho_m l a, \quad \Delta T_{13} = \Delta T_0 - m_{em} a, \quad \Delta T_{12} = \Delta T_{13} - \rho_m l_7 a,\\
&\Delta T_{11} = \Delta T_{12} - m_l a, \quad \Delta T_{10} = \Delta T_{11} - \rho_m l_6 a, \quad \Delta T_9 = \Delta T_{10} - m_l a,\\
&\Delta T_8 = \Delta T_9 - \rho_m l_5 a.
\end{aligned} \tag{34}$$

Since $T_{ia} = T_{iv} + \Delta T_i$, where $i = 0, 1, \ldots, 13$ and the corresponding tensions T_{iv} during constant velocity movement have been calculated earlier, the tensions T_{ia} at the two ends of all the band segments during acceleration can be determined from Eqs. (33) and (34). The tension at any other point in each band segment varies linearly along its length. The prototype and model tensions T_{0a} under the movement profiles in Figs. 4 and 5 are shown in Figs. 3(a) and (b), respectively. While the two tensions have similar trends, they are not completely analogous for two reasons. First, the prototype and model elevators have different configurations: an open loop in the prototype and a closed loop in the inverted model. Second, the two systems have different frictions. Whereas the prototype tension increases and decreases by 7.6% during acceleration and deceleration in regions 2 and 6 (see Table 4), respectively, the model tension increases by 12.4–13.1% in region 2 and decreases by 20.4–21.1% in region 6. While the prototype tension remains constant during constant velocity movement in region 4, the model tension decreases from 143.6 N to 141.7 N. Note that the change in the model tension due to acceleration depends on the position of the motor pulley and relative band lengths. The motor is placed in its current position because it can be easily accessed during experiments and because the resulting model tension has a similar trend to that of the prototype.

When the band slips on the motor pulley, the friction force between them develops a tension ratio in the band across the pulley equaling [9]

$$\frac{T_7}{T_8} = e^{\mu\phi}, \tag{35}$$

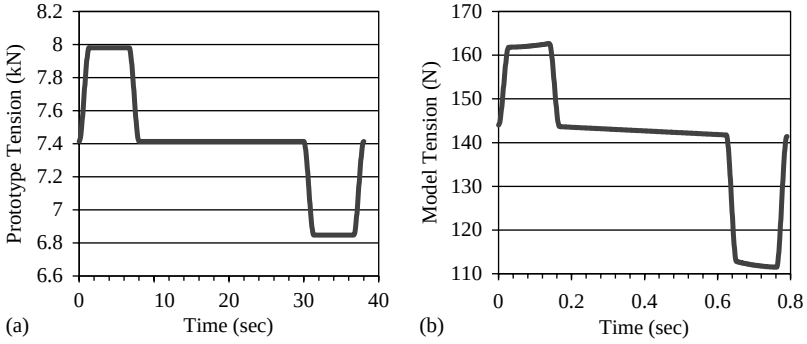

Fig. 3. The prototype (a) and model (b) tensions at the top of the car under the movement profiles shown in Figs. 4 and 5, respectively.

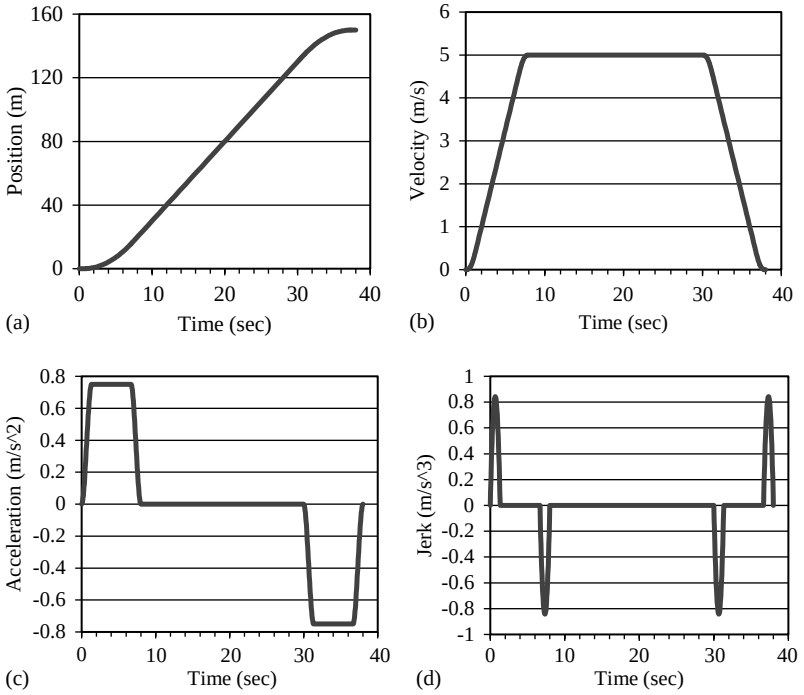

Fig. 4. The calculated position (a), velocity (b), acceleration (c), and jerk (d) functions for the prototype elevator using the times and polynomial coefficients in Table 5.

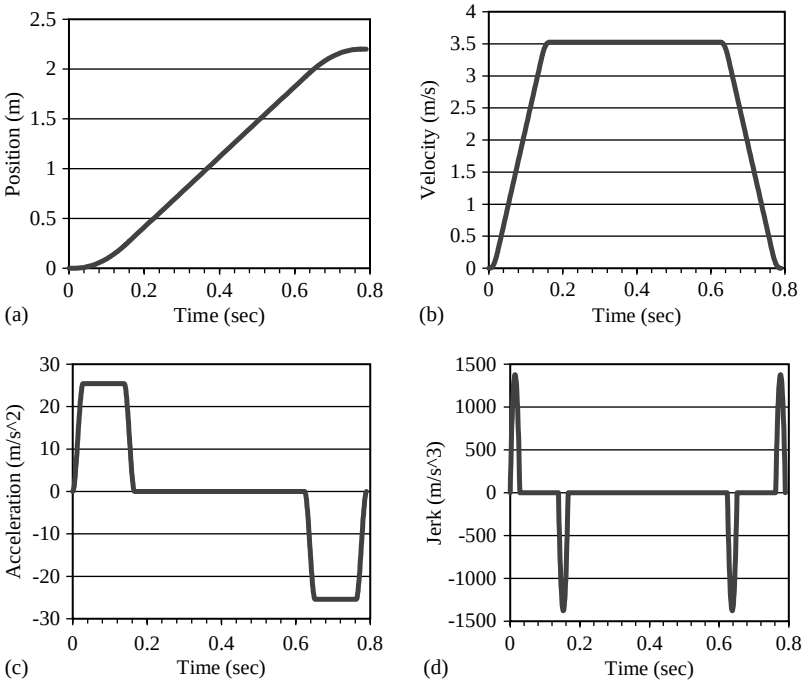

Fig. 5. The calculated position (a), velocity (b), acceleration (c), and jerk (d) functions for the model elevator using the times and polynomial coefficients in Table 6.

Table 4
Movement profile regions and descriptions

Movement region	Description
1	Increasing acceleration to $a = a_{maxp}$
2	Constant acceleration at a_{maxp}
3	Decreasing acceleration to $a = 0$, $v = v_{maxp}$
4	Constant velocity at v_{maxp}
5	Increasing deceleration to $a = -a_{maxp}$
6	Constant deceleration at $a = -a_{maxp}$
7	Decreasing deceleration to $a = 0$, $v = 0$, $p = 150\,\text{m}$

where μ is the coefficient of friction between the band and pulley and ϕ is the angle of wrap of the band around the pulley. The maximum tension ratio across the motor pulley occurs at the start of region 2, when $T_7 = 179\,\text{N}$ and $T_8 = 123\,\text{N}$. Because the band wraps an angle of 2.39 rad around the motor pulley, the minimum coefficient of friction required to prevent band slip is 0.16. Since the typical coefficients of friction between the motor pulley and band range from 0.07 to 0.12, the model exhibited considerable slip. In order to control band slip, the motor pulley was coated with a plastic substance used to coat tool handles. The coating, which can last about 200 runs before it needs to be reapplied, performs well and very little slip was observed. Increasing the wrap angle ϕ around the motor pulley would also reduce band slip.

6. Design and scaling of the movement profile

Given the maximum velocity v_{maxp}, maximum acceleration a_{maxp}, and final position l_{0p} of the prototype elevator, a movement profile can be created. In order to reduce the vibration caused by an instantaneous change in acceleration (infinite jerk), the movement profile developed has a continuous and finite jerk throughout the entire period of motion. The position function of the elevator, defined by $p(t_p) = l_{0p} + l_{endp} - l(t_p)$, is divided into seven regions as shown in Table 4. Let t_{0p} be the start time of region 1, and t_{1p} through t_{7p} be the times at the ends of regions 1–7, respectively. Similarly, let p_0 through p_7, v_0 through v_7, a_0 through a_7, and j_0 through j_7 be the positions, velocities, accelerations, and jerks at times t_{0p} through t_{7p}, respectively. In each region i (i=1, 2, …, 7), the position function is given by a fifth order polynomial

$$p(t_p) = C_{0p}^{(i)} + C_{1p}^{(i)}(t_p - t_{(i-1)p}) + C_{2p}^{(i)}(t_p - t_{(i-1)p})^2 + C_{3p}^{(i)}(t_p - t_{(i-1)p})^3 + C_{4p}^{(i)}(t_p - t_{(i-1)p})^4 + C_{5p}^{(i)}(t_p - t_{(i-1)p})^5, \tag{36}$$

where $t_{(i-1)p} \leqslant t_p \leqslant t_{ip}$ and $C_{np}^{(i)}$ $(n = 0,1, \ldots, 5)$ are unknown constants to be determined. A symmetric movement profile is designed here, which requires that the duration of region 1 equal those of regions 3, 5, and 7, and the duration of region 2 equal that of region 6. The durations of regions 1, 3, 5, and 7 are set to be a fraction β of the total acceleration ($t_{3p} - t_{0p}$) or deceleration ($t_{7p} - t_{4p}$) time:

$$t_{1p} - t_{0p} = t_{3p} - t_{2p} = t_{5p} - t_{4p} = t_{7p} - t_{6p} = \beta(t_{3p} - t_{0p}) = \beta(t_{7p} - t_{4p}), \tag{37}$$

where $0 \leqslant \beta \leqslant 0.5$. By adjusting β, we can indicate how much of the total acceleration or deceleration time is spent changing the acceleration, which will affect the maximum jerk value. When $\beta = 0$, the durations of regions 1, 3, 5, and 7 vanish, resulting in a discontinuous acceleration (infinite jerk) and a shortest flight time t_7. When $\beta = 0.5$, the durations of constant acceleration regions 2 and 6 vanish, resulting in smallest jerk values and a longest flight time.

Since the elevator starts from position $p = 0$ with zero velocity, acceleration, and jerk, we have $C_{0p}^{(1)} = C_{1p}^{(1)} = C_{2p}^{(1)} = C_{3p}^{(1)} = 0$. So in region 1,

$$p(t_p) = C_{4p}^{(1)}(t_p - t_{0p})^4 + C_{5p}^{(1)}(t_p - t_{0p})^5. \tag{38}$$

Differentiating Eq. (38) yields

$$\begin{aligned} v(t_p) &= 4C_{4p}^{(1)}(t_p - t_{0p})^3 + 5C_{5p}^{(1)}(t_p - t_{0p})^4, \\ a(t_p) &= 12C_{4p}^{(1)}(t_p - t_{0p})^2 + 20C_{5p}^{(1)}(t_p - t_{0p})^3, \\ j(t_p) &= 24C_{4p}^{(1)}(t_p - t_{0p}) + 60C_{5p}^{(1)}(t_p - t_{0p})^2, \end{aligned} \tag{39}$$

where $j(t_p) = d^3p(t_p)/dt_p^3$ is the jerk. Since $t_{1p} - t_{0p} = \beta(t_{3p} - t_{0p})$, at the end of region 1, we have

$$\begin{aligned} p_1 &= C_{4p}^{(1)}\beta^4(t_{3p} - t_{0p})^4 + C_{5p}^{(1)}\beta^5(t_{3p} - t_{0p})^5, \\ v_1 &= 4C_{4p}^{(1)}\beta^3(t_{3p} - t_{0p})^3 + 5C_{5p}^{(1)}\beta^4(t_{3p} - t_{0p})^4, \\ a_1 &= a_{maxp} = 12C_{4p}^{(1)}\beta^2(t_{3p} - t_{0p})^2 + 20C_{5p}^{(1)}\beta^3(t_{3p} - t_{0p})^3, \\ j_1 &= 0 = 24C_{4p}^{(1)}\beta(t_{3p} - t_{0p}) + 60C_{5p}^{(1)}\beta^2(t_{3p} - t_{0p})^2. \end{aligned} \tag{40}$$

Region 2 is constant acceleration, so $C_{3p}^{(2)} = C_{4p}^{(2)} = C_{5p}^{(2)} = 0$ and the position function is

$$p(t_p) = C_{0p}^{(2)} + C_{1p}^{(2)}(t_p - t_{1p}) + C_{2p}^{(2)}(t_p - t_{1p})^2. \tag{41}$$

Differentiating Eq. (41) and applying the continuity of p, v, a, and j at time t_{1p} yields

$$C_{0p}^{(2)} = p_1, \quad C_{1p}^{(2)} = v_1, \quad C_{2p}^{(2)} = \frac{a_{maxp}}{2}. \tag{42}$$

Since $t_{2p} - t_{1p} = (1 - 2\beta)(t_{3p} - t_{0p})$, at the end of region 2 we have

$$\begin{aligned} p_2 &= p_1 + v_1(1 - 2\beta)(t_{3p} - t_{0p}) + \frac{a_{maxp}}{2}(1 - 2\beta)(t_{3p} - t_{0p})^2, \\ v_2 &= v_1 + a_{maxp}(1 - 2\beta)(t_{3p} - t_{0p}) \end{aligned} \tag{43}$$

and

$$a_2 = a_{maxp}, \quad j_2 = 0. \tag{44}$$

Region 3 is similar to region 1. The coefficients $C_{0p}^{(3)}$ through $C_{3p}^{(3)}$ can be found by using the continuity conditions of p, v, a, and j at time t_{2p}:

$$C_{0p}^{(3)} = p_2, \quad C_{1p}^{(3)} = v_2, \quad C_{2p}^{(3)} = \frac{a_{maxp}}{2}, \quad C_{3p}^{(3)} = 0. \tag{45}$$

The position function in region 3 is then given by

$$p(t_p) = p_2 + v_2(t_p - t_{2p}) + \frac{a_{maxp}}{2}(t_p - t_{2p})^2 + C_{4p}^{(3)}(t_p - t_{2p})^3 + C_{4p}^{(3)}(t_p - t_{2p})^4 + C_{5p}^{(3)}(t_p - t_{2p})^5. \quad (46)$$

At the end of region 3, the velocity is v_{maxp}, and the acceleration and jerk are zero. Also, the duration of region 3 is the same as that of region 1, i.e., $t_{3p} - t_{2p} = \beta(t_{3p} - t_{0p})$. So at the end of region 3, we have

$$\begin{aligned} p_3 &= p + v_2\beta(t_{3p} - t_{0p}) + \frac{a_{maxp}}{2}\beta^2(t_{3p} - t_{0p})^2 + C_{4p}^{(3)}\beta^4(t_{3p} - t_{0p})^4 + C_{5p}^{(3)}\beta^5(t_{3p} - t_{0p})^5, \\ v_3 &= v_{\max p} = v_2 + a_{maxp}\beta(t_{3p} - t_{0p}) + 4C_{4p}^{(3)}\beta^3(t_{3p} - t_{0p})^3 + 5C_{5p}^{(3)}\beta^4(t_{3p} - t_{0p})^4, \\ a_3 &= 0 = a_{maxp} + 12C_{4p}^{(3)}\beta^2(t_{3p} - t_{0p})^2 + 20C_{5p}^{(3)}\beta^3(t_{3p} - t_{0p})^3, \\ j_3 &= 0 = 24C_{4p}^{(3)}\beta(t_{3p} - t_{0p}) + 60C_{5p}^{(3)}\beta^2(t_{3p} - t_{0p})^2. \end{aligned} \quad (47)$$

There are 10 equations in Eqs. (40), (43) and (47) with 10 unknowns: $C_{4p}^{(1)}, C_{5p}^{(1)}, t_{3p}, p_1, v_1, p_2, v_2, p_3, C_{4p}^{(3)}$ and $C_{5p}^{(3)}$. Solving these equations yields

$$\begin{aligned} C_{4p}^{(1)} &= -C_{4p}^{(3)} = \frac{a_{maxp}}{4\beta^2(t_{3p} - t_{0p})^2}, \quad C_{5p}^{(3)} = -C_{5p}^{(1)} = \frac{a_{maxp}}{10\beta^3(t_{3p} - t_{0p})^3}, \\ t_{3p} &= t_{0p} + \frac{v_{maxp}}{a_{maxp}(1-\beta)}. \end{aligned} \quad (48)$$

Region 4 is constant velocity, so $C_{2p}^{(4)} = C_{3p}^{(4)} = C_{4p}^{(4)} = C_{5p}^{(4)} = 0$. Since regions 5, 6, and 7 bring the velocity back to zero with the same times as regions 1, 2, and 3, the coefficients are

$$C_{4p}^{(5)} = C_{4p}^{(3)} = -C_{4p}^{(1)}, \quad C_{5p}^{(5)} = C_{5p}^{(3)} = -C_{5p}^{(1)}, \quad C_{4p}^{(7)} = C_{4p}^{(1)}, \quad C_{5p}^{(7)} = C_{5p}^{(1)}. \quad (49)$$

Region 6 is constant acceleration, so $C_{3p}^{(6)} = C_{4p}^{(6)} = C_{5p}^{(6)} = 0$. The other coefficients for regions 4–7 can be found by using the continuity conditions between the end of one region and the start of the next region. The only remaining unknown is t_{4p}. Since the acceleration and deceleration regions have the same durations and magnitudes, the distance travelled from t_{0p} to t_{3p} will equal that from t_{4p} to t_{7p}. So with $p_7 = 150\,\text{m}$ and p_3 determined from the first equation in Eq. (47), we have

$$t_{4p} = t_{3p} + \frac{p_7 - 2p_3}{v_{maxp}}. \quad (50)$$

Based on observations of an actual acceleration profile from the elevator industry [10], we choose $t_{2p} = 4t_{1p}$, and hence $\beta = \frac{1}{6}$. With $t_{0p} = 0$ the times at the ends of all the regions, along with the polynomial coefficients in each region, are shown in Table 5. The resulting position, velocity, acceleration, and jerk curves for the prototype elevator are shown in Fig. 4. It is seen that the maximum jerk falls under the range specified by the elevator industry.

The movement profile for the model is given by the same polynomials as those for the prototype in all the regions with different times and coefficients. The corresponding times and polynomial coefficients for the model are obtained by multiplying those for the prototype by appropriate combinations of l_0, ρ, and T_0 for the model and prototype:

$$t_{im} = t_{ip}\frac{l_{0m}}{l_{0p}}\sqrt{\frac{\rho_m T_{0p}}{\rho_p T_{0m}}}, \quad C_{nm}^{(i)} = C_{np}^{(i)}\frac{l_{0m}}{l_{0p}}\left(\frac{l_{op}}{l_{0m}}\sqrt{\frac{\rho_p T_{0m}}{\rho_m T_{0p}}}\right)^n, \quad (51)$$

Table 5
Prototype movement profile times and polynomial coefficients

Region i	t_{ip} (s)	$C_{0p}^{(i)}$ (m)	$C_{1p}^{(i)}$ (m/s)	$C_{2p}^{(i)}$ (m/s^2)	$C_{3p}^{(i)}$ (m/s^3)	$C_{4p}^{(i)}$ (m/s^4)	$C_{5p}^{(i)}$ (m/s^5)
1	1.33	0	0	0	0	0.106	−0.0316
2	6.67	0.2	0.5	0.375	0	0	0
3	8	13.5	4.5	0.375	0	−0.106	0.0316
4	30	20	5	0	0	0	0
5	31.33	130	5	0	0	−0.106	0.0316
6	36.67	136.5	4.5	−0.375	0	0	0
7	38	149.8	0.5	−0.375	0	0.106	−0.0316

Table 6
Model movement profile times and polynomial coefficients

Region i	t_{im} (s)	$C_{0m}^{(i)}$ (m)	$C_{1m}^{(i)}$ (m/s)	$C_{2m}^{(i)}$ (m/s^2)	$C_{3m}^{(i)}$ (m/s^3)	$C_{4m}^{(i)}$ (m/s^4)	$C_{5m}^{(i)}$ (m/s^5)
1	0.028	0	0	0	0	8277	−119430
2	0.139	0.003	0.35	12.72	0	0	0
3	0.166	0.198	3.17	12.72	0	−8277	119430
4	0.624	0.293	3.53	0	0	0	0
5	0.651	1.907	3.53	0	0	−8277	119430
6	0.762	2.002	3.17	−12.72	0	0	0
7	0.790	2.197	0.35	−12.72	0	8277	−119430

where $n = 0,1, \ldots, 5$. The calculated times for the model at the ends of all the regions, along with the polynomial coefficients in each region, are shown in Table 6. The resulting position, velocity, acceleration, and jerk curves for the model are shown in Fig. 5. Unlike the prototype elevator that transports humans, there are no limits to the maximum acceleration and jerk allowed for the model other than the hardware constraints.

7. Numerical solution

The accuracy of the model in representing the dynamic response of the prototype can be assessed numerically. The lateral vibrations of both the prototype and model cables under consideration are described by Eq. (1) with boundary conditions

$$y(0,t) = y_x(0,t) = y(l(t),t) = y_x(l(t),t) = 0. \tag{52}$$

The tension in Eq. (1) is rewritten as

$$T(x,t) = T_{0a}(t) + \rho[eg - \ddot{l}(t)][l(t) - x], \tag{53}$$

where $T_{0a}(t) = m_e[g - \ddot{l}(t)]$ for the prototype and $T_{0a}(t)$ is calculated as shown in Section 5.2 for the model, and $e = 1$ for the prototype and $e = -1$ for the model. By modified Galerkin's

method [5], the solution of Eqs. (1) and (52) is expressed in the form

$$y(x,t)=\sum_{i=1}^{n} q_i(t)\phi_i(x,t), \tag{54}$$

where $\phi_i(x,t)$ are the instantaneous orthonormal eigenfunctions of an untensioned, stationary beam with variable length $l(t)$ and fixed boundaries, n is the number of included modes, and q_i are the generalized coordinates. A key observation here, similar to that in Ref. [5], is that $\phi_i(x,t)$ can be expressed as

$$\phi_i(x,t)=\frac{1}{\sqrt{l(t)}}\psi_i(\xi), \tag{55}$$

where $\xi=\dfrac{1}{\sqrt{l(t)}}$, and $\psi_i(\xi)$, as given in Appendix B, are the orthonormal eigenfunctions of an untensioned, stationary beam with unit length and fixed boundaries. While the governing equation in Eq. (1) is based on the Eulerian description of motions of the translating cables, their lateral velocity in the Eulerian or Lagrangian frame of reference can be calculated. In the former, the local velocity of the cable particle, passing through a spatial position x at time t, is

$$y_t(x,t)=\sum_{i=1}^{n}\left[-\frac{1}{2}l^{-\frac{3}{2}}(t)\dot{l}(t)q_i(t)+l^{-\frac{1}{2}}(t)\dot{q}_i(t)\right]\psi_i\left(\frac{x}{l(t)}\right)-\sum_{i=1}^{n} xl^{-\frac{5}{2}}(t)\dot{l}(t)q_i(t)\psi_i'\left(\frac{x}{l(t)}\right). \tag{56}$$

In the latter, the inertial velocity of a fixed cable particle, located at position x at time t, is

$$\begin{aligned}\frac{\mathrm{D}y(x,t)}{\mathrm{D}t}&=y_t(x,t)+\dot{l}(t)y_x(x,t)=\sum_{i=1}^{n}\left[-\frac{1}{2}l^{-\frac{3}{2}}(t)\dot{l}(t)q_i(t)+l^{-\frac{1}{2}}(t)\dot{q}_i(t)\right]\psi_i\left(\frac{x}{l(t)}\right)\\&\quad+\sum_{i=1}^{n}\left[l^{-\frac{3}{2}}(t)-xl^{-\frac{5}{2}}(t)\right]\dot{l}(t)q_i(t)\psi_i'\left(\frac{x}{l(t)}\right),\end{aligned} \tag{57}$$

where $\dfrac{\mathrm{D}}{\mathrm{D}t}$ is referred to as the material time derivative.

Substituting Eqs. (54) and (55) into Eq. (1), multiplying the resulting expression by $\dfrac{1}{\sqrt{l(t)}}\psi_k\left(\dfrac{x}{l(t)}\right)$, and integrating it from $x=0$ to $l(t)$, yields the discretized equations of motion of the translating cables with time-varying coefficients:

$$\mathbf{M}(t)\ddot{\mathbf{q}}(t)+\mathbf{G}(t)\dot{\mathbf{q}}(t)+[\mathbf{K}(t)+\mathbf{H}(t)]\mathbf{q}(t)=0, \tag{58}$$

where $\mathbf{q}=[q_1,q_2,\ldots,q_n]^{\mathrm{T}}$ is the vector of generalized coordinates, $\mathbf{M}$ and $\mathbf{K}$ are the symmetric mass and stiffness matrices, and $\mathbf{G}$ and $\mathbf{H}$ are the skew-symmetric gyroscopic and circulatory matrices. Entries of these matrices are given in Appendix B. Note that the presence of the car mass m_e does not introduce an equivalent damping matrix in Eq. (58), as is the case in references [5,6], because of the fixed boundary conditions here at $x=l(t)$. Since all the integrals that involve the trial functions in the entries of system matrices are time-independent, dependence of system matrices on time appears only in the coefficients of their component matrices, which greatly simplifies the analysis. If the initial displacement and velocity of the cables are specified by $y(x,0)$ and $y_t(x,0)$,

respectively, the initial values for $\mathbf{q}$ and $\dot{\mathbf{q}}$ are [5]

$$q_i(0) = \sqrt{l(0)} \int_0^1 y(\xi l(0), 0)\psi_i(\xi)\,\mathrm{d}\xi, \tag{59}$$

$$\dot{q}_i(0) = \sqrt{l(0)} \int_0^1 y_t(\xi l(0), 0)\psi_i(\xi)\,\mathrm{d}\xi + \frac{v(0)}{l(0)} \sum_{k=1}^{n} q_k(0) \int_0^1 \xi\psi_k(\xi)\psi_i(\xi)\,\mathrm{d}\xi + \frac{v(0)}{2l(0)} q_i(0). \tag{60}$$

The discretized expression of the energy associated with lateral vibration of the cables is [5]

$$E(t) = \tfrac{1}{2}[\dot{\mathbf{q}}^{\mathrm{T}}(t)\mathbf{M}(t)\dot{\mathbf{q}}(t) + \dot{\mathbf{q}}^{\mathrm{T}}(t)\mathbf{R}(t)\dot{\mathbf{q}}(t) + \mathbf{q}^{\mathrm{T}}(t)\mathbf{S}(t)\mathbf{q}(t)], \tag{61}$$

where entries of matrices $\mathbf{R}$ and $\mathbf{S}$ are given in Appendix B. Eq. (58) is integrated numerically using the initial conditions in Eqs. (59) and (60). While an elevator cable can be modeled as a translating string [5], the prototype and model cables are modeled here as a translating, tensioned beam, in order to include the effects of bending rigidity on their dynamic responses. The prototype and model cables have small dimensionless bending rigidity, and a large number of terms are retained in Eq. (54). While the results are not shown here, convergence is achieved for the prototype and model cables in the following example when $n = 30$.

Let the initial displacement of the prototype cable be

$$y(x, 0) = 16 y_{maxp} \left(\frac{x}{l_{0p}}\right)^2 \left(1 - \frac{x}{l_{0p}}\right)^2, \quad 0 < x < l_{0p}, \tag{62}$$

where $y_{maxp} = 0.068$ m is the maximum displacement at the center of the cable, and the initial velocity along the cable is set to zero. The lateral displacement and velocity of a fixed particle on the cable, located at a distance of 14.18 m above the top of the car (i.e., $x = l(t) - 14.18$ m), are shown as solid lines in Figs. 6(a), (b), and the energy of vibration of the cable is shown as a solid line in Fig. 6(c). Under the initial displacement of the model band, corresponding to that of the prototype cable in Eq. (62),

$$y(x, 0) = 16 y_{maxm} \left(\frac{x}{l_{0m}}\right)^2 \left(1 - \frac{x}{l_{0m}}\right)^2, \quad 0 < x < l_{0m}, \tag{63}$$

where $y_{maxm} = \dfrac{l_{0m}}{l_{0p}} y_{maxp} = 1$ mm, and zero initial velocity, the lateral displacement and velocity of a corresponding fixed particle on the band, located at a distance of 0.21 m away from the top of the car (i.e., $x = l(t) - 0.21$ m), are calculated, along with the energy of vibration of the segment of the band under consideration. By multiplying the model variables by appropriate combinations of l_0, ρ, and T_0 for the model and prototype, the model responses are converted to those of the prototype that the model represents, as shown in dashed lines in Fig. 6. Though the model is not fully scaled with the prototype, its dynamic response closely resembles that of the prototype. With $E_p(t)$ denoting the energy of vibration of the prototype cable and $E_m(t)$ the energy of vibration predicted from the model, as shown in Fig. 6(c), the error defined by

$$\varepsilon = \frac{\|E_m(t) - E_p(t)\|}{\|E_p(t)\|} \times 100\%, \tag{64}$$

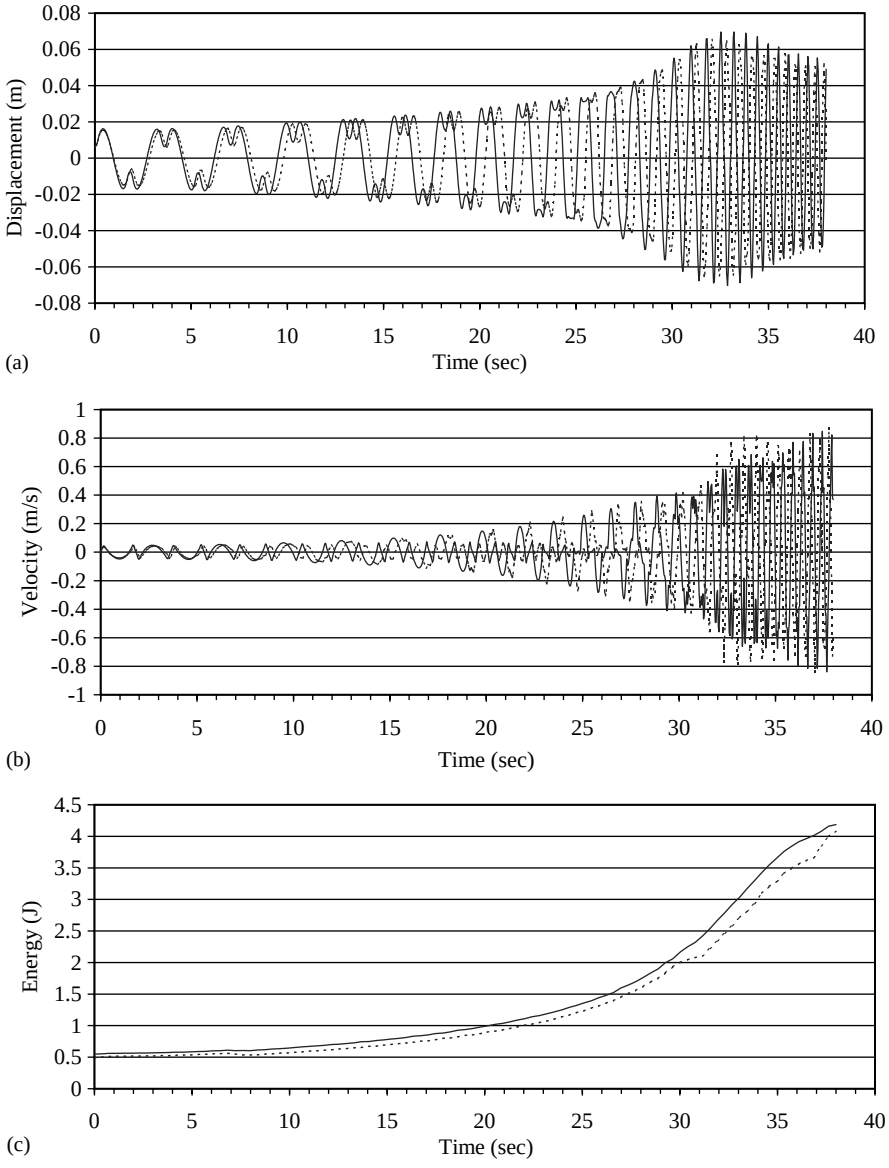

Fig. 6. The actual (solid) and predicted (dashed) responses of the prototype cable with $n=30$ and the time domain divided into 1000 intervals. The lateral displacement and velocity of a fixed particle on the cable, located at $x=l(t)-14.18$ m, are shown in (a) and (b), respectively, and the energy of vibration of the cable is shown in (c).

where $\|\cdot\|$ is the L_2-norm evaluated in the entire period of motion from $t=0$–38 s, is calculated to be 9.2%. While the model band has a relatively larger dimensionless bending rigidity, and a larger increase and decrease of tension during acceleration and deceleration phases of motion, respectively, the prototype cable has a larger increase of tension due to its own weight. The

effective stiffness, and consequently, the energy of vibration of the prototype are seen to be higher than those represented by the model. While the amplitudes of the displacements in Fig. 6(a) increase first and decrease near the ends of travel, the energies of vibration in Fig. 6(c) increase in general during retraction of the cables, a phenomenon termed as the "unstable shortening cable behavior" [5].

8. Concluding remarks

While it is impossible to obtain a fully scaled model unless the model is extremely tall, a model of more practical size is developed using a closed band loop. Numerical results show that the model has the same behavior as the prototype and can predict its response with errors less than 10%. All the scaling laws are satisfied except those associated with the bending rigidity (Π_7), the tension change due to cable weight (Π_8), and the tension change due to acceleration (Π_9). The effect of these three pi terms on the scaling between the model and prototype is minimized. While the current model was designed for the prototype described in Section 2, by adjusting the model tension and movement profile it can be used to simulate the lateral dynamics of a different prototype cable.

Acknowledgements

This work is supported by the National Science Foundation through the award number CMS-0116425. The authors would like to thank all the undergraduate students for their assistance in the design and fabrication of the scaled elevator model. They would also like to thank Dr. Randy Roberts at Otis Elevator Company for his support on this work.

Appendix A

Effects of bending rigidity on the natural frequencies of prototype and model cables

The degrees to which the prototype and model cables behave like an ideal string can be estimated by calculating their natural frequencies using both the beam and string models. The maximum differences between the natural frequencies from the two models, which occur at the ends of elevator movements, are obtained. The tension changes due to cable weights are not considered here because they have a maximum value of 2.8%. The natural frequencies (in Hz) of a cable of length l_{end}, modelled as a tensioned beam with pinned ends, are given by [11]

$$f_i = \sqrt{\frac{i^2 T_0}{4\rho l_{end}^2} + \frac{i^4 \pi^2 EI}{4\rho l_{end}^4}}, \tag{A.1}$$

where $i \in \mathbb{N}$. The natural frequencies (in Hz) of the cable modelled as a tensioned beam with fixed ends are obtained from [8]

$$\frac{T_0}{4\pi f_i\sqrt{\rho EI}}\sin(s_2 l_{end}) - \cos(s_2 l_{end}) - 2e^{-s_1 l_{end}} - \mathrm{e}^{-2s_1 l_{end}}\left(\frac{T_0}{4\pi f_i\sqrt{\rho EI}}\sin(s_2 l_{end}) + \cos(s_2 l_{end})\right) = 0, \tag{A.2}$$

where

$$s_1 = \sqrt{\sqrt{\frac{T_0^2}{4(EI)^2} + \frac{4\pi^2\rho f_i^2}{EI}} + \frac{T_0}{2EI}}, \quad s_2 = \sqrt{\sqrt{\frac{T_0^2}{4(EI)^2} + \frac{4\pi^2\rho f_i^2}{EI}} - \frac{T_0}{2EI}}. \tag{A.3}$$

Note that to avoid the numerical difficulties in evaluating the hyperbolic functions with large arguments, the frequency equation in Eq. (A.2) is expressed in terms of exponential functions with negative exponents. When $EI = 0$ the natural frequencies in Eq. (A.1) correspond to those of a fixed–fixed string. Since the natural frequencies of a tensioned beam with pinned ends fall between those of a string and a tensioned beam with fixed ends, the first five natural frequencies of the latter two cases are calculated using the prototype and model parameters in Tables 1 and 2 and shown in Tables 7 and 8, respectively. It is seen that relatively higher dimensionless bending rigidity of the model has a larger effect on higher frequency modes.

Appendix B

Trial functions and entries of matrices in Section 7

The orthonormal eigenfunctions of an untensioned, stationary beam with unit length and fixed boundaries are [11]

$$\psi_i(\xi) = \beta_i[\cosh\kappa_i\pi\xi - \cos\kappa_i\pi\xi - \sigma_i(\sinh\kappa_i\pi\xi - \sin\kappa_i\pi\xi)], \quad 0 \leqslant \xi \leqslant 1, \tag{B.1}$$

where κ_i is the ith positive root of the transcendental equation

$$\cos\kappa_i\pi\cosh\kappa_i\pi = 1 \tag{B.2}$$

Table 7
Natural frequencies of the prototype cable at its end of movement predicted from the beam and string models

Mode number	Beam model frequency (Hz)	String model frequency (Hz)	Percent difference
1	1.624	1.621	0.2
2	3.248	3.242	0.2
3	4.872	4.863	0.2
4	6.496	6.485	0.2
5	8.121	8.106	0.2

Table 8
Natural frequencies of the model band at its end of movement predicted from the beam and string models

Mode number	Beam model frequency (Hz)	String model frequency (Hz)	Percent difference
1	108.1	101.0	6.5
2	219.1	202.0	7.8
3	335.8	303.0	9.8
4	460.8	404.0	12.3
5	596.2	505.0	15.3

and

$$\sigma_i = \frac{\cosh\kappa_i\pi - \cos\kappa_i\pi}{\sinh\kappa_i\pi - \sin\kappa_i\pi}, \tag{B.3}$$

$$\beta_i = \sqrt{\kappa_i\pi}\{(1+\sigma_i^2)[\tfrac{1}{4}\sinh 2\kappa_i\pi - \cosh\kappa_i\pi\sin\kappa_i\pi] + (1-\sigma_i^2)[\tfrac{1}{4}\sin 2\kappa_i\pi - \sinh\kappa_i\pi\cos\kappa_i\pi] + \kappa_i\pi + 2\sigma_i[\tfrac{1}{4}(\cos 2\kappa_i\pi - \cosh 2\kappa_i\pi) + \sin\kappa_i\pi\sinh\kappa_i\pi]\}^{-\frac{1}{2}}. \tag{B.4}$$

Since a large number of modes are included in the numerical solution, to avoid loss of precision in evaluating the hyperbolic functions with large arguments, Eq. (B.1) is rewritten as

$$\psi_i(\xi) = \beta_i\{-\cos\kappa_i\pi\xi + \sigma_i\sin\kappa_i\pi\xi + \frac{1}{1-e^{-2\kappa_i\pi}-2e^{-\kappa_i\pi}\sin\kappa_i\pi}[e^{-\kappa_i\pi\xi} - e^{-\kappa_i\pi(2-\xi)} + (\cos\kappa_i\pi - \sin\kappa_i\pi)e^{-\kappa_i\pi(1-\xi)} - (\sin\kappa_i\pi + \cos\kappa_i\pi)e^{-\kappa_i\pi(1+\xi)}]\}. \tag{B.5}$$

When $i > 5$, $\kappa_i = (i+0.5)\pi$ and $\sigma_i = \beta_i = 1$.

Entries of system matrices in Eq. (58) are given by

$$M_{ki} = \rho\delta_{ki}, \tag{B.6}$$

$$G_{ki} = -2\rho l^{-1}(t)\dot{l}(t)\left[\frac{1}{2}\delta_{ki} - \int_0^1 (1-\xi)\psi_i'(\xi)\psi_k(\xi)\,d\xi\right], \tag{B.7}$$

$$K_{ki} = \frac{1}{4}\rho l^{-2}(t)\dot{l}^2(t)\delta_{ki} - \rho l^{-2}(t)\dot{l}^2(t)\int_0^1 (1-\xi)^2\psi_k'(\xi)\psi_i'(\xi)\,d\xi + \rho l^{-1}(t)[eg - \ddot{l}(t)]\int_0^1 (1-\xi)\psi_k'(\xi)\psi_i'(\xi)\,d\xi + T_{0a}(t)l^{-2}(t)\int_0^1 \psi_k'(\xi)\psi_i'(\xi)\,d\xi + EIl^{-4}(t)\int_0^1 \psi_k''(\xi)\psi_i''(\xi)\,d\xi, \tag{B.8}$$

$$H_{ki} = \rho[l^{-2}(t)\dot{l}^2(t) - l^{-1}(t)\ddot{l}(t)]\left[\frac{1}{2}\delta_{ki} - \int_0^1 (1-\xi)\psi_k(\xi)\psi_i(\xi)\,d\xi\right], \tag{B.9}$$

where δ_{ki} is the Kronecker delta. Entries of matrices **R** and **S** in Eq. (61) are

$$R_{ki} = -\rho l^{-1}(t)\dot{l}(t)\delta_{ki} + 2\rho l^{-1}(t)\dot{l}(t)\int_0^1 (1-\xi)\psi_k(\xi)\psi_i'(\xi)\,d\xi, \tag{B.10}$$

$$S_{ki} = \rho\left[-\frac{1}{4}l^{-2}(t)\dot{l}^2(t)\delta_{ki} + \dot{l}^2(t)l^{-2}(t)\int_0^1 (1-\xi)^2\psi_k'(\xi)\psi_i'(\xi)\,\mathrm{d}\xi + l^{-1}(t)[eg - \ddot{l}(t)]\int_0^1 (1-\xi)\psi_k'(\xi)\psi_i'(\xi)\,\mathrm{d}\xi\right] + EIl^{-4}(t)\int_0^1 \psi_k''(\xi)\psi_i''(\xi)\,\mathrm{d}\xi + T_{0a}(t)l^{-2}(t)\int_0^1 \psi_k'(\xi)\psi_i'(\xi)\,\mathrm{d}\xi. \tag{B.11}$$

References

[1] R. Roberts, Control of high-rise/high-speed elevators, Proceedings of the American Control Conference, FM16-1, Philadelphia, 1998.

[2] R.M. Chi, H.T. Shu, Longitudinal vibration of a hoist rope coupled with the vertical vibration of an elevator car, Journal of Sound and Vibration 148 (1) (1991) 154–159.

[3] T. Yamamoto, K. Yasuda, M. Kato, Vibrations of a string with time-variable length, Bulletin of the Japan Society of Mechanical Engineers 21 (162) (1978) 1677–1684.

[4] Y. Terumichi, M. Ohtsuka, M. Yoshizawa, Y. Fukawa, Y. Tsujioka, Nonstationary vibrations of a string with time-varying length and a mass–spring system attached at the lower end, Nonlinear Dynamics 12 (1997) 39–55.

[5] W.D. Zhu, J. Ni, Energetics and stability of translating media with an arbitrarily varying length, American Society of Mechanical Engineers Journal of Vibration and Acoustics 122 (2000) 295–304.

[6] W.D. Zhu, J. Ni, J. Huang, Active control of translating media with arbitrarily varying length, American Society of Mechanical Engineers Journal of Vibration and Acoustics 123 (2001) 347–358.

[7] F.M. White, Fluid Mechanics, 3rd Edition, McGraw-Hill, New York, 1994, pp. 260–266.

[8] L.J. Teppo, Experiments on Active Control of Vibration of an Elevator Cable with Varying Length, M.S.Thesis, University of North Dakota, 1999.

[9] A.H. Burr, J.B. Cheatham, Mechanical Analysis and Design, 2nd Edition, Prentice-Hall, Englewood Cliffs, Upper Saddle River, NJ, 1995, pp. 137–141.

[10] Performance Standards Committee, Vertical Transportation Standards, 7th Edition, Supplement, National Elevator Industry, Inc., Ft. Lee, NJ, 1994.

[11] S.S. Rao, Mechanical Vibrations, 3rd Edition, Addison-Wesley, Reading, MA, 1995, pp. 536–537.